Structure-based relaxation analysis reveals C-terminal [1-13C]glycine-*d₂* in peptides has long spin-lattice relaxation time that is applicable to *in vivo* hyperpolarized magnetic resonance studies

Yohei Kondo,[1] Yutaro Saito,[1] Tomohiro Seki,[2,†] Yoichi Takakusagi,[3,4] Jumpei Morimoto,[1] Hiroshi Nonaka,[1,‡] Koichiro Miyanishi,[5,6] Wataru Mizukami,[3,6] Makoto Negoro,[3,6] Abdelazim Elsayed Elhelaly,[7] Fuminori Hyodo,[7] Masayuki Matsuo,[8] Natarajan Raju,[9] Rolf Swenson,[9] Murali C. Krishna,[2] Kazutoshi Yamamoto,[2] and Shinsuke Sando[1,10,*]

[1]Department of Chemistry and Biotechnology, Graduate School of Engineering, The University of Tokyo, 7-3-1 Hongo, Bunkyo-ku, Tokyo 113-8656, Japan

[2]Center for Cancer Research, National Cancer Institute, National Institutes of Health, Bethesda, Maryland 20892, USA

[3]Quantum Hyperpolarized MRI Group, Institute for Quantum Life Science (iQLS), National Institutes for Quantum Science and Technology (QST), Anagawa 4-9-1, Inage, Chiba-city 263-8555, Japan

[4]Institute for Quantum Medical Science (iQMS), National Institutes for Quantum Science and Technology (QST), Anagawa 4-9-1, Inage, Chiba-city 263-8555, Japan

[5]Graduate School of Engineering Science, Osaka University, 1-3 Machikaneyama, Toyonaka, Osaka 560-8531, Japan

[6]Center for Quantum Information and Quantum Biology, Osaka University, Osaka 560-8531, Japan

[7]Department of Radiology, Frontier Science for Imaging, School of Medicine, Gifu University, 1-1 Yanagido, Gifu 501-1194, Japan

[8]Department of Radiology, School of Medicine, Gifu University, 1-1 Yanagido, Gifu 501-1194, Japan

[9]Chemistry and Synthesis Center, National Heart, Lung, and Blood Institute, National Institutes of Health, Rockville, MD 20850, USA.

[10]Department of Bioengineering, Graduate School of Engineering, The University of Tokyo, 7-3-1 Hongo, Bunkyo-ku, Tokyo 113-8656, Japan

[†]Present address: Faculty of Pharmacy and Pharmaceutical Sciences, Josai University, Keyakidai, Sakado, Saitama 350-0295, Japan

[‡]Present address: Department of Synthetic Chemistry and Biological Chemistry, Graduate School of Engineering, Kyoto University, Katsura, Nishikyo-ku, 615-8510, Japan

*Contact corresponding author

Prof. Dr. Shinsuke Sando

Department of Chemistry and Biotechnology, Graduate School of Engineering, The University of Tokyo

7-3-1 Hongo, Bunkyo-ku, Tokyo 113-8656, Japan

Email: ssando@chembio.t.u-tokyo.ac.jp

Abstract

Dissolution-dynamic nuclear polarization (d-DNP) is a state-of-the-art technology that can dramatically enhance the detection sensitivity of nuclear magnetic resonance (NMR). DNP NMR has been applied to small molecules with stable isotopes and has been used to obtain metabolic and physiological information *in vivo*. However, the hyperpolarized state exponentially decays back to the thermal equilibrium state, depending on the spin-lattice relaxation time (T_1). This signal decay has remained a major problem associated with this technology. Therefore, DNP NMR molecular probes useful for *in vivo* analysis have been limited to naturally occurring small molecules that inherently show long T_1. While peptides are promising targets for DNP NMR studies, because of the limitation in T_1, DNP NMR molecular probes applicable *in vivo* have been limited to amino acids or dipeptides. Herein we propose a [1-^{13}C]Gly-d_2 residue for realizing long T_1 in peptides. Structure-based T_1 relaxation analysis of amino acids and peptides revealed that (1) T_1 does not decrease monotonically with increasing molecular weight and (2) T_1 is not significantly affected by a side chain on the neighboring amino acid residue. These findings suggest that the C-terminal [1-^{13}C]Gly-d_2 residue affords sufficiently long T_1 for biological uses, even in oligopeptides, and allowed us to develop ^{13}C-β-casomorphin-5 (Tyr-Pro-Phe-Pro-[1-^{13}C]Gly-d_2, $T_1 = 24 \pm 4$ s at 3 T in H$_2$O) and ^{13}C-glutathione (γ-Glu-Cys-[1-^{13}C]Gly-d_2, $T_1 = 58 \pm 3$ s at 3 T in H$_2$O) as DNP NMR probes with long T_1. We succeeded in *in vivo* detection of enzymatic conversions of these two probes. These results demonstrate the utility of our strategy and would contribute to further expansion of the substrate scope for DNP applications.

Introduction

One of the more advanced methods for *in vivo* metabolic analysis is the combination of nuclear magnetic resonance (NMR) and dissolution-dynamic nuclear polarization (d-DNP), which is a technique that dramatically improves the NMR sensitivity of nuclei. By applying the DNP process to stable isotope-labeled molecular probes, typically ^{13}C-labeled molecular probes including ^{13}C-pyruvate, the NMR sensitivities can be enhanced as much as 10^3–10^5 times.[1] These highly sensitive hyperpolarized molecular probes allow us to obtain various information on metabolic activities and physiological parameters *in vivo* by ^{13}C magnetic resonance spectroscopy (MRS) or ^{13}C magnetic resonance imaging (MRI), which are expected to be applied to the early diagnosis of diseases and understanding of biological phenomena.[2–4]

However, hyperpolarization has a critical problem in that the highly sensitive NMR signal decays exponentially to that in thermal equilibrium with the spin-lattice relaxation time (T_1) as a time constant. Because of this limitation, molecular probes used for *in vivo* metabolic analyses have been limited to naturally occurring molecules containing ^{13}C nuclei with inherently long T_1. Various approaches have been used to design molecules with long T_1. One attempt is to use the ^{15}N nucleus, which has a smaller gyromagnetic ratio and thus longer T_1 than ^{13}C, and is thus expected to be applied to biological DNP MR studies.[5–9] Another approach involves deuteration to replace the nearby ^{1}H, which is the main T_1 relaxation source of the molecules.[10–15] Despite these approaches, molecules useful for *in vivo* applications are still limited. To further expand the scope of metabolic reactions and physiological parameters detectable *in vivo*, it is necessary to increase the repertoire of DNP NMR molecular probes. More specifically, it is necessary to understand the molecular mechanism of T_1 relaxation and to uncover the molecular structures that show long T_1 sufficient for *in vivo* DNP MR studies.

The spin relaxation rate of a nucleus, $R_1 = 1/T_1$, can be regarded as the sum of contributions from independent relaxation mechanisms.[16] Among them, relaxations due to ^{1}H-^{13}C dipole-dipole (DD) interaction and the symmetric part of chemical shift anisotropy (CSA) are the main relaxation factors for ^{13}C of small molecules under a high magnetic field. Therefore, in this study, relaxation mechanisms are classified into ^{1}H-^{13}C DD interaction, CSA relaxation, and a component related to all other relaxations (Other) including scalar coupling, spin rotation, and relaxation by paramagnetic agents such as dissolved oxygen, radical species, and metals, as shown in **Equation (1)**.

$$\frac{1}{T_1} = R_1 = R_{1DD} + R_{1CSA} + R_{1Other} \tag{1}$$

R_{1DD} and R_{1CSA} can be expressed using parameters that depend on the molecular structures and the environment, as shown in **Equations (2)** and **(3)**.[17]

$$R_{1DD} = \frac{\gamma_H{}^2 \gamma_C{}^2 \hbar^2}{r^6} \tau_2 \tag{2}$$

$$R_{1CSA} = \frac{2}{15} \gamma_C{}^2 B_0{}^2 \Delta\sigma^2 (3 + \eta^2) \tau_2 \tag{3}$$

where γ is the gyromagnetic ratio of the nuclei, $\hbar$ is Dirac's constant, r is the distance between ^{1}H and ^{13}C of interest, τ_2 is the second rotational correlation time, B_0 is the strength of the external magnetic field, $\Delta\sigma$ is the chemical shift

anisotropy, and η is the asymmetry parameter. Among these parameters, τ_2 is related to molecular motion and is generally known to be positively correlated with the size of the molecule.[18] As shown in **Equations (2)** and **(3)**, there is a linear correlation between τ_2 and the relaxations due to DD and CSA. In addition, large molecules generally have a large number of ^{1}H nuclei, resulting in an increase in DD interactions. Therefore, larger molecules typically tend to show shorter T_1.[19,20] Because of this relationship between the size of molecules and T_1, it has been believed difficult to achieve the T_1 applicable *in vivo* for molecules with large molecular weights (molecular weight > 200). To the best of our knowledge, *in vivo* metabolic analysis using ^{13}C-labeled molecular probes with a molecular weight of over 200 has rarely been performed except for diethyl α-[1-^{13}C]ketoglutarate (molecular weight = 203) and γ-glutamyl[1-^{13}C]glycine (molecular weight = 205).[19–22]

Peptides, which are composed of amino acids, are promising targets for *in vivo* hyperpolarized MR analysis because they undergo sequence-specific reactions and modifications. Moreover, peptides participate in biological phenomena by interacting with various proteins. Therefore, there is a growing interest in detecting and tracking the metabolism, localization, and *in vivo* dynamics of peptides.[23] However, because the average molecular weight of natural amino acids is 110, even the dipeptides have an average molecular weight of over 200, and the molecular weight of tripeptides usually exceeds 300. Thus, peptides larger than trimers are thought to be unsuitable for *in vivo* hyperpolarized metabolic analysis because of the negative correlation between molecular weight and T_1. Indeed, amino acid/peptide-type DNP NMR probes that have achieved *in vivo* metabolic measurements to date are only γ-glutamyl[1-^{13}C]glycine (T_1 = 30 s, 9.4 T,)[22], N-acetyl[1-^{13}C]cysteine (T_1 = 20 s, 3 T)[24], [1-^{13}C]alanine (T_1 = 29 s, 9.4 T)[25], [6-^{13}C,^{15}N$_3$]arginine (T_1 = 7.2 s, 14.1 T; T_1 = 15 s, 1 T)[26], [^{13}C]glutamine (C1: T_1 = 25 s, 9.4 T, C5: T_1 = 16 s, 9.4 T)[25,27–29], [1-^{13}C]glutamate (T_1 = 34 s, 9.4 T)[30], and [1-^{13}C]alanine ethyl ester (T_1 = 64 s, 3 T)[31], which are monomers or dimers (**Figure 1A, B**).

Herein we propose a ^{13}C-labeling strategy to utilize oligopeptides as DNP NMR molecular probes with long T_1 values applicable to *in vivo* studies (**Figure 1A**). Our strategy is based on the following findings: (1) T_1 does not decrease monotonically with increasing molecular weight, and (2) T_1 is not significantly affected by a side chain on the neighboring amino acid residue. By experimentally and computationally interpreting these findings based on the molecular mechanism underlying T_1 relaxation, the C-terminal [1-^{13}C]Gly-d_2 residue was found to be suitable for long T_1 in peptides (**Figure 1A**). We demonstrated the biologically applicable T_1 of ^{13}C in the tripeptide, glutathione (GSH) with the sequence of γ-Glu-Cys-Gly, which has a molecular weight of > 300, and even in the pentapeptide, β-casomorphin-5 (Tyr-Pro-Phe-Pro-Gly), which has a molecular weight exceeding 500. These long T_1 enabled *in vivo* hyperpolarized metabolic observation of the peptides (**Figure 1B**).
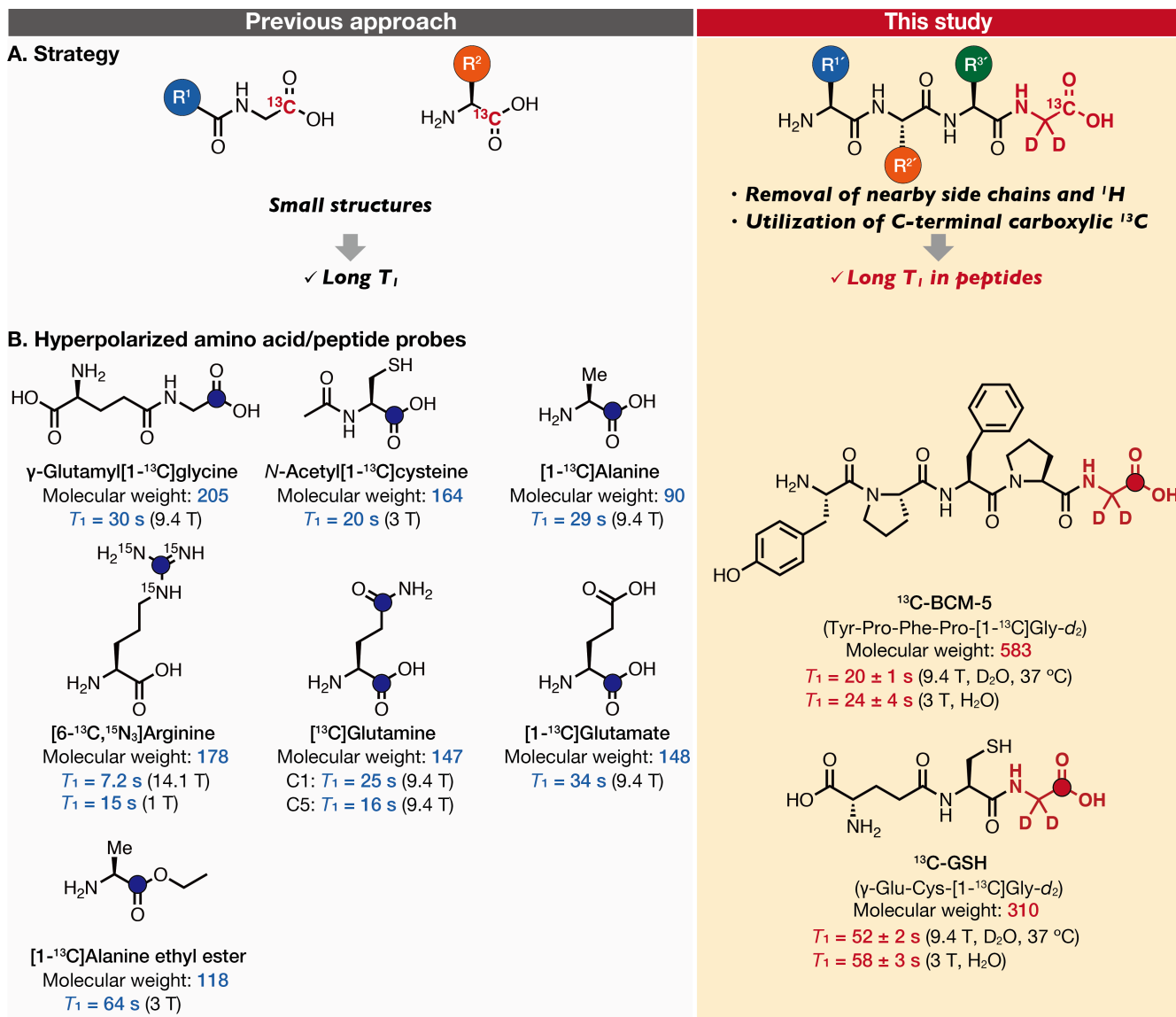
Figure 1. (A) The conceptual illustration comparing the previous approach with this study to realize a long spin-lattice relaxation time (T_1) in amino acids or peptides. (B) ^{13}C-amino acids and peptides that have been used for *in vivo* hyperpolarized MR studies are shown in the left side. Shown in the right side are the peptide-based DNP NMR molecular probes that are developed in this study. T_1 values of γ-glutamyl[1-^{13}C]glycine, *N*-acetyl[1-^{13}C]cysteine, [1-^{13}C]alanine, [6-^{13}C,[15]N$_3$]arginine, [^{13}C]glutamine, [1-^{13}C]glutamate, and [1-^{13}C]alanine ethyl ester were cited from ref. 22, 24, 25, 26, 27, 30, and 31. Colored atoms indicate isotope-enriched [13]C.

Results and Discussion

T_1 relaxation effect of main chain length on peptides

T_1 analysis of glycine oligomers

To elucidate the relationship between T_1 and the main chain length of peptides, we first investigated T_1 values of C-terminal carboxylic ^{13}C nuclei and amide ^{13}C nuclei at the second residue from the C-terminus using glycine oligomers as model peptides. In 2009, D. M. Wilson *et al*. reported that the T_1 values of an acetyl moiety in *N*-acetyldiglycine and an acetyl moiety of the lysine side chain in *N,N′*-diacetyllysylprolylvaline are 9.8 s and 9.5 s, respectively.[32] They implicated that the relationship between molecular weight and T_1 is not exact because *N,N′*-diacetyllysylprolylvaline, with a 2-fold larger molecular weight than *N*-acetyldiglycine, showed almost the same T_1 value. This result suggests that even peptides with large molecular weights may exhibit long T_1 values that are applicable to *in vivo* analysis. We were inspired to investigate the relationship between the peptide main chain length and T_1.

Two sets of glycine oligomers (n = 2–5), with a ^{13}C nucleus at the C-terminal carboxylic acid or the amide carbonyl group of the second residue from the C-terminus, were prepared (**Figure 2A and Scheme S1**). The T_1 values of the model peptides and [1-^{13}C]Gly monomer were measured at 9.4 T using the saturation recovery method (**Figure 2B**). As expected, there is an approximate negative correlation between T_1 and the main chain length, i.e., the molecular weight. Focusing on the amide carbonyl group at the second residue from the C-terminus in glycine oligomers, the longer the main chain, the shorter the T_1. The T_1 value uniformly decreased, and in pentaglycine, T_1 was $12 \pm <1$ s (9.4 T, 5 mM, D$_2$O, 37 ºC), which was one-fourth of the T_1 value of the [1-^{13}C]Gly monomer (blue bars in **Figure 2B**).

On the other hand, we found that the T_1 of C-terminal carboxylic ^{13}C did not monotonously decrease with increasing molecular weight (red bars in **Figure 2B**). The T_1 of the trimer decreased to 32 ± 1 s; however, the rate of decrease was dramatically suppressed, and the T_1 of C-terminal carboxylic ^{13}C in pentaglycine remained at 24 ± 1 s (9.4 T, 5 mM, D$_2$O, 37 ºC). This experimental result suggests that T_1 is not determined simply by molecular weight, or rather, dependent on the molecular structure. In the case of larger peptides, the C-terminal carboxylic ^{13}C is suggested to be preferable to the amide carbonyl group to achieve long T_1.

To explain the above experimental results based on the molecular structures of glycine oligomers, we simulated T_1 of glycine oligomers using molecular dynamics and quantum mechanical calculations (**see Supporting Information**, **Table S1**).[33] The simulated T_1 values were within 24%–218% error compared with experimentally determined T_1 values, and the trends of T_1 values were well correlated between the experiments and simulations; therefore, this simulated data was used to evaluate the experimental results (**Tables S1, 2**). We first investigated the reason for the long T_1 of the C-terminal carboxylic ^{13}C by focusing on the second rotational correlation time (τ_2). The C-terminal carboxylic ^{13}C in glycine 3–5 mers showed almost the same τ_2 values (13.2–15.7 ps, **Table S1**). This simulated result suggests that the local molecular rotation around the C-terminal carboxylic ^{13}C is almost the same within glycine 3–5 mers. Considering that ^{1}H-^{13}C R_{1DD} and R_{1CSA} are dominated by τ_2, this may be one of the reasons for the experimental result that T_1 values of C-terminal carboxylic ^{13}C of glycine oligomers do not decrease as the molecular weight increases.

We then discuss the difference in T_1 between the intramolecular amide ^{13}C and the C-terminal carboxylic ^{13}C. Experimental T_1 analysis revealed that T_1 of the intramolecular amide ^{13}C of glycine oligomers decreased as the main chain lengthened, resulting in a smaller T_1 value than that of the C-terminal carboxylic ^{13}C (e.g., $12 \pm <1$ s versus 24 ± 1 s in pentaglycine, **Figure 2B**). The simulated τ_2 of amide ^{13}C (27.8 ps) was larger than that of the C-terminal carboxylic ^{13}C (15.7 ps) in pentaglycine. It may be possible to explain that this difference in τ_2 might be due to the intramolecular amide bond being less flexible than the C-terminal carboxylic group. In addition, the difference in τ_2 can be regarded as

one of the reasons for the smaller R_{1DD} and R_{1CSA}, resulting in longer T_1 of the C-terminal carboxylic ^{13}C. These results suggest that the C-terminal carboxylic ^{13}C nucleus in peptides can realize long T_1, and even large oligopeptides can potentially be used as DNP NMR molecular probes.

Hyperpolarized ^{13}C-heptaglycine to demonstrate the feasibility of a long T_1 in a peptide with a long main chain

We were motivated to examine the T_1 value of heptaglycine, which has a longer main chain. ^{13}C-heptaglycine (Gly$_6$-[1-^{13}C]Gly) was prepared by the solid-phase peptide synthesis method (**Scheme S1**). T_1 of C-terminal ^{13}C in heptaglycine was determined to be 24 ± 3 s (9.4 T, <1.25 mM, D$_2$O, 37 ºC, **Figure 2B**), which is interestingly almost the same as tetra- ($27 \pm <1$ s) and pentaglycine (24 ± 1 s). ^{13}C-heptaglycine was then subjected to hyperpolarization experiments using a Hypersense DNP polarizer and a 3 T MRI scanner. The mixture of ^{13}C-heptaglycine (*ca.* 0.24 M in DMSO/glycerol) containing OX063 (*ca.* 16 mM) as a polarizing agent was hyperpolarized for 2 h and rapidly dissolved by 3.5 mL of H$_2$O containing 200 mg/L EDTA disodium salt. The ^{13}C MRS was performed at 3 T. The hyperpolarized ^{13}C-heptaglycine gave an enhanced ^{13}C MR signal, and its hyperpolarized signal was observed over 60 s (**Figure 2C, D**). The corrected T_1 at 3 T was calculated as 22 s (3 T, H$_2$O). This result opens the possibility of ^{13}C-labeling at the C-terminal carboxylic group to achieve long T_1 and sufficient hyperpolarization lifetime in peptides.
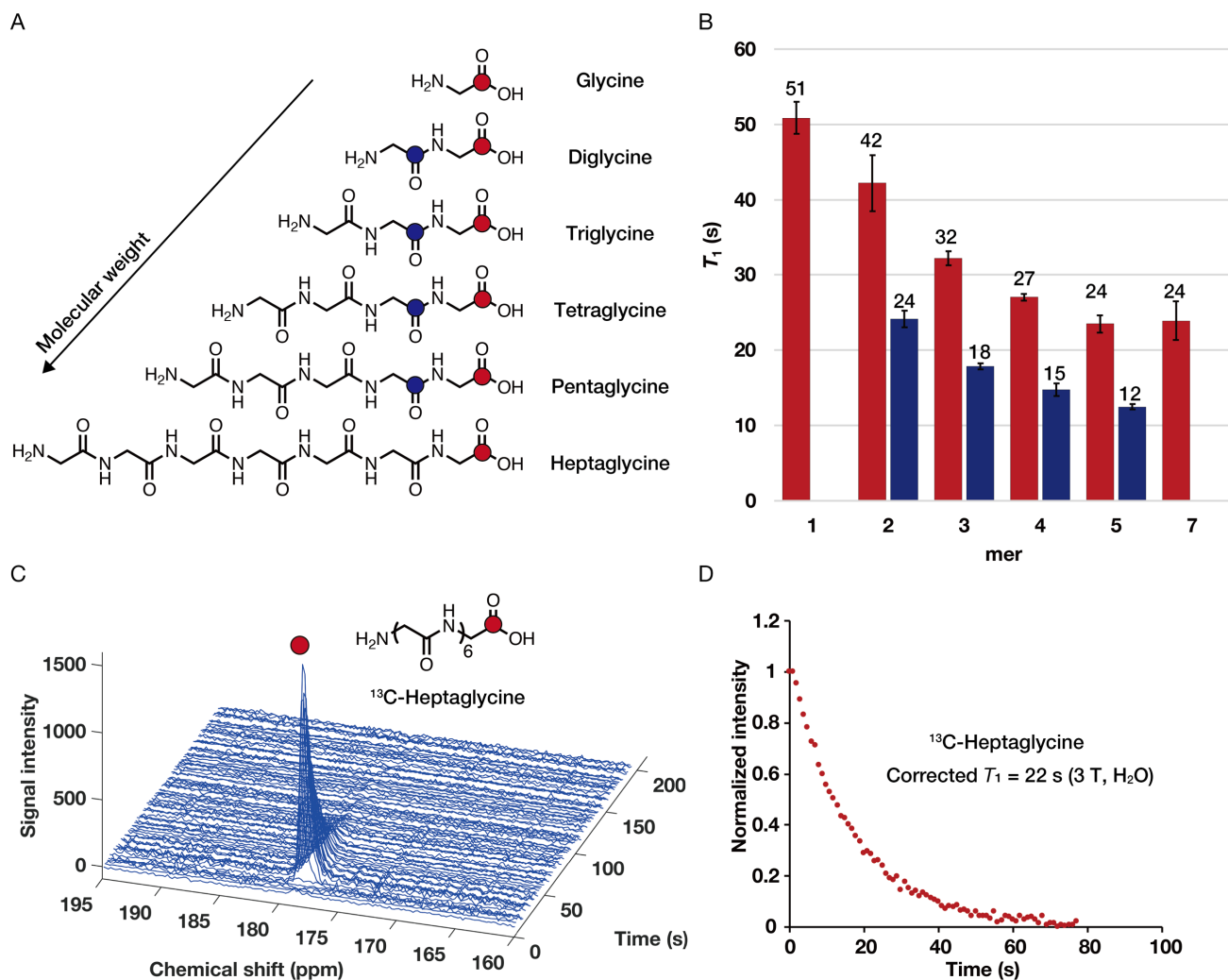
Figure 2. (A) Chemical structures of glycine oligomers. Red or blue-colored atoms are ^{13}C, whose T_1 values are measured. (B) T_1 values of glycine oligomers. T_1 values were measured using the saturation recovery method (9.4 T, 5 mM, D_2O, 37 ºC, pD = 7.4 ± 0.1) except for heptaglycine (9.4 T, <1.25 mM, D_2O, 37 ºC, pD = 7.4 ± 0.1). The color of bars corresponds to the color of ^{13}C nuclei in the chemical structures shown in (A). Error bars represent standard deviation (n = 3). (C) Dynamic ^{13}C MRS of hyperpolarized ^{13}C-heptaglycine (Gly$_6$-[1-^{13}C]Gly) was performed using a 3 T MRI scanner. 10 µL of ^{13}C-heptaglycine (*ca.* 0.24 M in DMSO/glycerol) containing OX063 (*ca.* 16 mM) was hyperpolarized using Hypersense. Repetition time = 1 s, flip angle = 10°, dissolution buffer was 3.5 mL of H_2O containing 200 mg/L EDTA disodium salt. 1.0 mL of hyperpolarized solution was added to a glass vial with 2.0 mL of H_2O containing 200 mg/L EDTA disodium salt. (D) Time course of hyperpolarized ^{13}C-heptaglycine signal. The corrected T_1 value at 3 T was calculated from the hyperpolarized signal decay considering the signal loss through acquisitions.

T_1 relaxation effect of side chains in peptides

T_1 analysis of [1-^{13}C]Xaa and Leu-[1-^{13}C]Xaa

We focus on the relationship between T_1 of peptides and side chains. To investigate the relationship between the size of the side chains and carboxylic ^{13}C in amino acid monomers, the T_1 values of [1-^{13}C]Gly, [1-^{13}C]Ala, [1-^{13}C]Val, [1-^{13}C]Ser, [1-^{13}C]Leu, [1-^{13}C]Phe, and [1-^{13}C]Lys were measured. As a result, the T_1 values of carboxylic ^{13}C tended to become shorter as the side chain became larger (**Figure 3A**).

We then examined the relationship between the size of the side chains and T_1 of the C-terminal carboxylic ^{13}C of dipeptides using Leu-[1-^{13}C]Xaa (Xaa = Gly, Ala, and Leu, **Figure 3B**). We first confirmed that the T_1 values of these dipeptides decreased as the side chains became larger. T_1 values of C-terminal carboxylic ^{13}C in Leu-[1-^{13}C]Xaa (Xaa = Gly, Ala, and Leu) were determined to be 31 ± <1 s, 24 ± 1 s, and 16 ± 1 s, respectively (9.4 T, 10 mM, D$_2$O, 37 ºC, **Figure 3B**). These dipeptides also showed the same tendency of T_1 as amino acid monomers, where T_1 decreased as the side chain became larger.
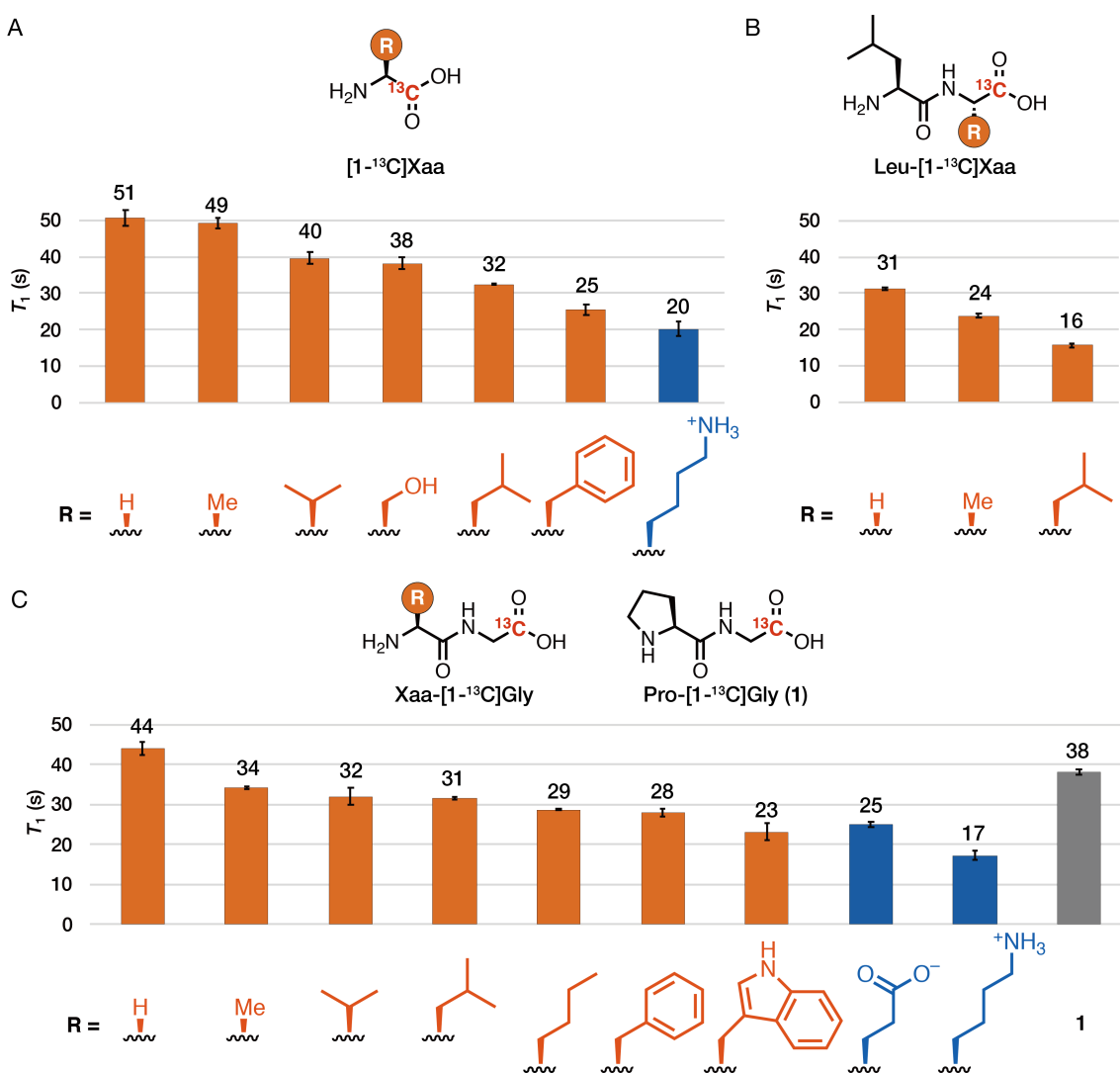
Figure 3. (A) Chemical structures and T_1 values of [1-^{13}C]Xaa. Xaa = Gly, Ala, Val, Ser, Leu, Phe, and Lys. Non-polar and polar side chains are colored orange and blue, respectively. (B) Chemical structures and T_1 values of Leu-[1-^{13}C]Xaa. Xaa = Gly, Ala, and Leu. (C) Chemical structures and T_1 values of Xaa-[1-^{13}C]Gly. Xaa = Gly, Ala, Val, Leu, Nle, Phe, Trp, Glu, Lys, and Pro. All T_1 values were measured using the saturation recovery method (9.4 T, 10 mM, D$_2$O, 37 ºC, pD = 7.4 ± 0.1). Error bars represent standard deviation (n = 3).

R_1 analysis of Leu-[1-^{13}C]Gly and Gly-[1-^{13}C]Leu

To obtain more precise insights into the above experimental results on the T_1 relaxation effect of side chains, we analyzed T_1, R_{1DD}, and R_{1CSA} of Leu-[1-^{13}C]Gly and Gly-[1-^{13}C]Leu as model dipeptides, especially focusing on the position of the side chains. We first experimentally determined T_1 values of Leu-[1-^{13}C]Gly and Gly-[1-^{13}C]Leu at 9.4 T (**Figure 4A**). Leu-[1-^{13}C]Gly, which does not have a side chain directly attached to the ^{13}C residue, showed a longer T_1 of 31 ± <1 s (9.4 T, 10 mM, D$_2$O, 37 ºC) than Gly-[1-^{13}C]Leu (21 ± <1 s). By simply changing the position of the side chain, Leu-[1-^{13}C]Gly showed 1.5-fold longer T_1 than the dipeptide with the same molecular weight, i.e., Gly-[1-^{13}C]Leu.

To interpret the T_1 relaxation mechanism realizing the longer T_1 of Leu-[1-^{13}C]Gly, we first focused on ^{1}H-^{13}C DD relaxation. ^{1}H-^{13}C R_{1DD} was determined experimentally by a method utilizing nuclear Overhauser effect.[14,34–38] The ^{1}H-^{13}C R_{1DD} of Gly-[1-^{13}C]Leu and Leu-[1-^{13}C]Gly were 17.1 × 10^{-3} s^{-1} and 15.0 × 10^{-3} s^{-1}, respectively (**Figure 4A, S1**). To obtain a more detailed explanation of these experimental results based on the molecular structures, we simulated T_1 of Leu-[1-^{13}C]Gly and Gly-[1-^{13}C]Leu in D$_2$O using molecular dynamics and quantum mechanical calculations (**see Supporting Information, Table S3**).[33] The T_1 values of Leu-[1-^{13}C]Gly and Gly-[1-^{13}C]Leu obtained in the simulations were within an error of 35% from those obtained experimentally, and the trends in T_1 values correlated well between the experiment and the simulations (**Table S4**). The R_{1DD} contribution of each ^{1}H in the dipeptides, obtained from the simulations, is shown in **Figure 4B**. For Gly-[1-^{13}C]Leu, R_{1DD} of α-^{1}H of the Leu residue and ^{1}H in the side chain were simulated to account for 76% and 24% of the contribution of ^{1}H-^{13}C R_{1DD}. Regarding Leu-[1-^{13}C]Gly, over 99% of the ^{1}H-^{13}C R_{1DD} contribution was suggested to be due to α-^{1}Hs of the Gly residue, while ^{1}Hs of the N-terminal Leu residue accounted for less than 1%. R_{1DD} analysis of the model dipeptides suggests that the side chain of the neighboring amino acid residue has only a small intramolecular ^{1}H-^{13}C DD relaxation effect on the C-terminal carboxylic ^{13}C.

Next, we focused on CSA relaxation: R_{1CSA} analysis of Leu-[1-^{13}C]Gly and Gly-[1-^{13}C]Leu. In the case of the model dipeptides, assuming that the magnetic field dependence of the relaxation mechanisms other than CSA was small enough to be ignored, R_{1CSA} of Leu-[1-^{13}C]Gly and Gly-[1-^{13}C]Leu can be determined experimentally by examining the external magnetic field dependence of T_1 (**Figure 4A, S2**).[14,39,40] R_{1CSA} of Gly-[1-^{13}C]Leu was 14.5 × 10^{-3} s^{-1}, which was larger than Leu-[1-^{13}C]Gly (9.75 × 10^{-3} s^{-1}). We then conducted R_{1CSA} simulations to understand the experimental results. The simulated R_{1CSA} of Gly-[1-^{13}C]Leu was also larger than Leu-[1-^{13}C]Gly, which is consistent with the experimental results (**Table S4**). However, the calculated values of chemical shift anisotropy for Leu-[1-^{13}C]Gly (90.70 ppm) and Gly-[1-^{13}C]Leu (95.75 ppm) were almost the same, suggesting that the difference in R_{1CSA} between Leu-[1-^{13}C]Gly and Gly-[1-^{13}C]Leu resulted from the difference in τ_2, as indicated by **Equation (3)**. The simulated τ_2 value of the C-terminal carboxylic ^{13}C in Leu-[1-^{13}C]Gly (17.7 ps) was smaller than Gly-[1-^{13}C]Leu (28.4 ps). Given that τ_2 is involved in molecular motions, the difference in the flexibility of the C-terminal carboxylic groups may be the factor that induces the difference in τ_2 between Leu-[1-^{13}C]Gly and Gly-[1-^{13}C]Leu.

To gain insight into the flexibility of the C-terminal carboxylic groups of the model dipeptides, diagrams of preferable conformations for the dihedral angles ϕ and ψ of the C-terminal residues of Leu-[1-^{13}C]Gly and Gly-[1-^{13}C]Leu were generated using the molecular dynamics trajectories. While the diagram of Gly-[1-^{13}C]Leu showed only two major conformations: $(\phi, \psi) = (-81°, 135°)$ and $(\phi, \psi) = (-36°, -63°)$, the diagram of Leu-[1-^{13}C]Gly showed several preferable conformations, suggesting that the C-terminal carboxylic group of Leu-[1-^{13}C]Gly can form more diverse structures than that of Gly-[1-^{13}C]Leu (**Figure 4C**). Next, we plotted the time-dependent fluctuation of the dihedral angle ψ of the C-terminal residues of the model dipeptides from the trajectory (**Figure 4D, S3**). The plots showed that the dihedral angle ψ of the C-terminal [1-^{13}C]Gly residue in Leu-[1-^{13}C]Gly was less restricted than the C-terminal [1-^{13}C]Leu residue in

Gly-[1-^{13}C]Leu, supporting the more flexibility of the C-terminal carboxylic group of Leu-[1-^{13}C]Gly. These results suggest that the existence of a side chain near the C-terminal carboxylic ^{13}C restricts the molecular rotation of the carboxylic group. This restricted molecular rotation, in addition to other motions, may be one reason for the increase in τ_2, resulting in a larger R_{1CSA} of Gly-[1-^{13}C]Leu. The above experimental and simulation results for R_{1CSA} of the model dipeptides suggest that the C-terminal [1-^{13}C]Gly residue with no directly attached side chain is advantageous for the longer T_1 of peptides in terms of reducing not only DD relaxation but also CSA relaxation.
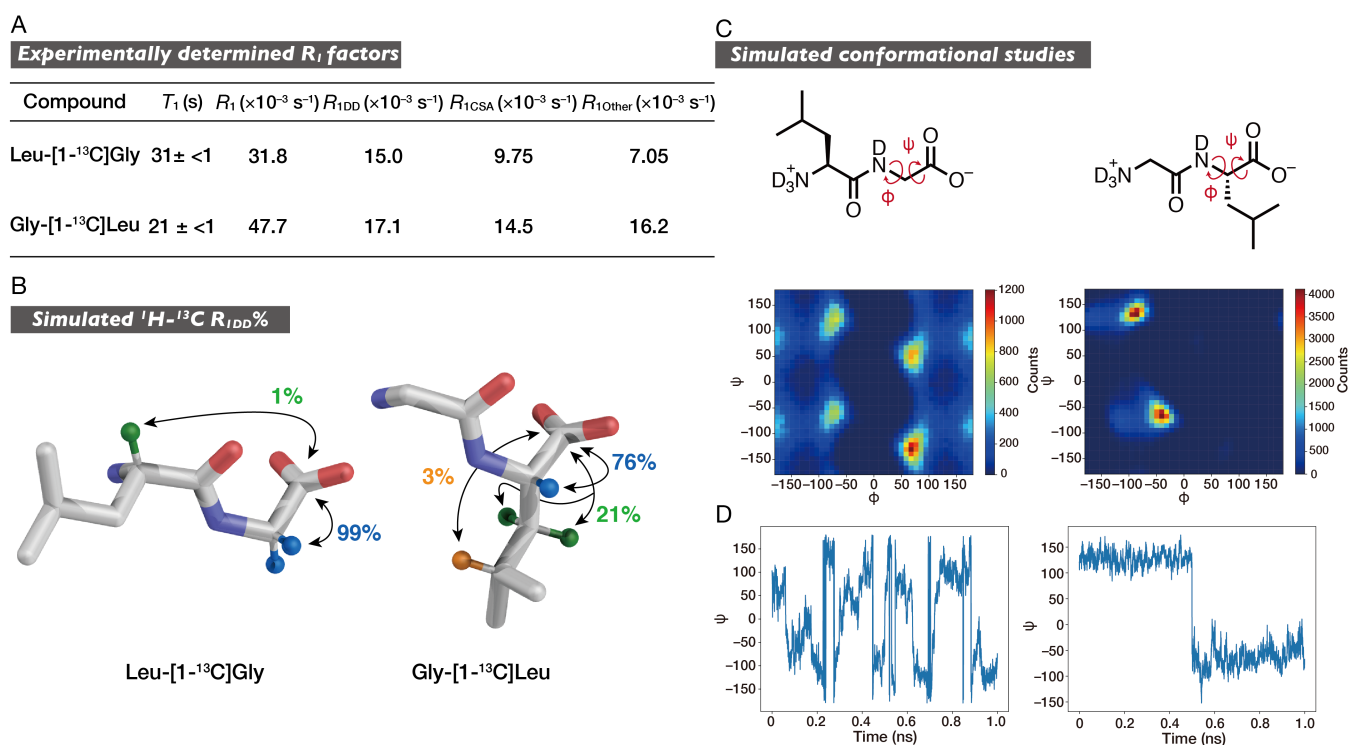
Figure 4. (A) Experimentally determined T_1 values and each R_1 contributions of Leu-[1-^{13}C]Gly and Gly-[1-^{13}C]Leu at 9.4 T in D$_2$O. (B) Simulated intramolecular ^{1}H-^{13}C R_{1DD} contribution of ^{1}Hs of Leu-[1-^{13}C]Gly and Gly-[1-^{13}C]Leu in D$_2$O. ^{1}Hs that are not shown with colored balls account for less than 1% of the intramolecular ^{1}H-^{13}C R_{1DD} contribution. Carbon, oxygen, and nitrogen are shown as gray, red, and blue sticks, respectively. (C) The diagrams showing the preferable conformations of Leu-[1-^{13}C]Gly (left) and Gly-[1-^{13}C]Leu (right), which were generated from the whole molecular dynamics trajectories. The dihedral angles ϕ and ψ of the C-terminal residues are used for the diagrams. (D) Time-dependent fluctuation of ψ of the C-terminal residues of Leu-[1-^{13}C]Gly (left) and Gly-[1-^{13}C]Leu (right). The calculations were run over 100.5 ns, and time-dependent fluctuations were plotted during 1 ns.

*T*₁ analysis of Xaa-[1-¹³C]Gly

T_1 **analysis of Xaa-[1-¹³C]Gly**

We then investigated the T_1 values of Xaa-[1-¹³C]Gly (Xaa = Gly, Ala, Val, Leu, Nle, Phe, Trp, Glu, Lys, and Pro) to validate the insight that T_1 of the C-terminal [1-¹³C]Gly residue is not significantly affected by a side chain on the neighboring amino acid residue. Xaa-[1-¹³C]Gly (Xaa = Gly, Ala, Val, Leu, Nle, Phe, Trp, Glu, Lys, and Pro) were prepared according to **Scheme S3** to determine their T_1 values. As expected, Xaa-[1-¹³C]Gly (Xaa = Ala, Val, Leu, Nle, Phe, Trp, and Glu) showed almost the same T_1 value at approximately 30 s, regardless of the size of its side chain (**Figure 3C**). The ¹H-¹³C DD relaxation, i.e., R_{1DD}, accounted for almost the same extent (37%–55%) of R_1 in these dipeptides (**Figure S4**). This result experimentally supports the hypothesis that intramolecular ¹H-¹³C DD relaxation caused by the ¹Hs of the side chain in Xaa-[1-¹³C]Gly does not significantly contribute to the T_1 relaxation of the C-terminal carboxylic ¹³C. In addition, Gly-[1-¹³C]Gly and Pro-[1-¹³C]Gly showed larger T_1 values of approximately 40 s. It was suggested that glycine and proline residues may be effective for longer T_1 of C-terminal carboxylic ¹³C in peptides. As an exception, Lys-[1-¹³C]Gly exhibited a smaller T_1 value than the other dipeptides. However, Lys-[1-¹³C]Gly still showed a T_1 value of approximately 20 s, and its T_1 value was almost the same as that of the [1-¹³C]Lys monomer. These experimental results for Xaa-[1-¹³C]Gly validated our insight that the C-terminal [1-¹³C]Gly residue is not significantly affected by a side chain on the neighboring amino acid residue and is preferable for long T_1 in peptides.

Proposal of ¹³C-labeling strategy for long *T*₁ in peptides

By combining the insights into T_1 relaxation of the side chain and the main chain discussed above, we propose a ¹³C-labeling strategy for peptides that utilizes C-terminal [1-¹³C]Gly-d_2 to realize long T_1. The following are the bases of this ¹³C-labeling strategy: First, ¹³C-labeling at the C-terminal carboxylic group is demonstrated to achieve long T_1 and sufficient hyperpolarization lifetime even in oligopeptides; Second, it is suggested that the C-terminal [1-¹³C]Gly residue is not significantly affected by a side chain on the neighboring amino acid residue and is preferable for reducing both R_{1DD} and R_{1CSA}; Finally, since the α-¹Hs of the [1-¹³C]Gly residue account for the majority of intramolecular ¹H-¹³C DD relaxation, α-deuteration can contribute to further elongation of T_1.

Development of ^{13}C-β-casomorphin-5 as a pentapeptide DNP NMR probe with a long T_1

Based on the ^{13}C-labeling strategy proposed above, we attempted to develop a peptide-based DNP NMR molecular probe for biological studies. β-Casomorphin-5 is a pentapeptide fragment digested from milk protein and is known to be a μ-opioid receptor agonist.[41] Its amino acid sequence is Tyr-Pro-Phe-Pro-Gly. Based on the ^{13}C-labeling strategy proposed herein, we designed and developed ^{13}C-BCM-5 (**2**) (Tyr-Pro-Phe-Pro-[1-^{13}C]Gly-d_2) as a DNP NMR molecular probe (**Figure 5A**). Peptide **2** was synthesized on the solid phase using Fmoc-[1-^{13}C]Gly-d_2 as the starting material, according to **Scheme S4**.

The C-terminal [1-^{13}C]Gly-d_2 residue in peptide **2** showed T_1 of 20 ± 1 s (9.4 T, 5 mM, D$_2$O, 37 ºC). This value was much larger than the T_1 values that pentapeptides were expected to have (**Table S5**). An enhanced ^{13}C MR signal of hyperpolarized peptide **2** was observed in dynamic ^{13}C MR spectra acquired using a 3 T MRI scanner (**Figure 5D**). From the hyperpolarized signal decays, the corrected T_1 at 3 T was calculated as 24 ± 4 s (3 T, H$_2$O), suggesting that peptide **2** can retain a sufficient hyperpolarized signal under aqueous conditions (**Figure S5**).

We then examined whether hyperpolarized peptide **2** could be used for monitoring enzymatic activity. In our bodies, β-casomorphin-5 is usually metabolized into smaller peptide fragments by dipeptidyl peptidase-IV (DPP-IV).[41] DPP-IV is one of the serine proteases responsible for the initial cleavage of glucagon-like peptide-1, which is known as an incretin hormone.[42,43] DPP-IV is also suggested as a biomarker for various cancers, including esophageal cancers.[44–46] DPP-IV preferably recognizes the second proline residue on the N-terminus of peptides and catalyzes the cleavage of its amide bond. Peptide **2** with Tyr-Pro-Phe-Pro-[1-^{13}C]Gly-d_2 is first metabolized by DPP-IV to produce Phe-Pro-[1-^{13}C]Gly-d_2. Thereafter, Phe-Pro-[1-^{13}C]Gly-d_2 undergoes the second cleavage of Phe-Pro from its sequence to give [1-^{13}C]Gly-d_2 (**3**) as the final product of DPP-IV-mediated reactions (**Figure 5A**). By using hyperpolarized peptide **2** as a probe and tracing the hyperpolarized **3** as a product, DPP-IV activity can be detected.

First, the DPP-IV detection ability of probe **2** was tested in a thermal equilibrium state. Probe **2** exhibited a ^{13}C NMR signal at 177 ppm in phosphate buffer (9.4 T, 37 ºC, **Figure S6**). Upon incubation with human DPP-IV, a new ^{13}C NMR signal appeared at 173 ppm (**Figure 5B, S6**). The new peak was assigned as product **3**, by comparison with an authentic sample (9.4 T, 37 ºC, **Figure S7**). When reacted with DPP-IV, probe **2** should also produce the intermediate Phe-Pro-[1-^{13}C]Gly-d_2 in addition to product **3**. However, the ^{13}C chemical shift of Phe-Pro-[1-^{13}C]Gly-d_2 was found to be the same as that of probe **2** (9.4 T, 37 ºC, **Figure S7**). Therefore, in this case, only the ^{13}C NMR peak of product **3** could be detected after the two-step enzymatic reaction with DPP-IV. Because the addition of a DPP-IV inhibitor (K579) suppressed the production of the distinct ^{13}C NMR signal of product **3**, it was suggested to be a DPP-IV-mediated reaction (**Figure 5C, S6**). These results indicate that peptide **2** works as a ^{13}C NMR probe for DPP-IV activity by detecting product **3**.

Next, we conducted *in vivo* analysis using hyperpolarized probe **2**. Hyperpolarized probe **2** was intravenously administered to a healthy nude mouse (Athymic NCr-nu/nu). Dynamic ^{13}C MR spectra were acquired from the mouse body region (**Figure 5E**). The appearance of a distinct ^{13}C MR peak was observed at the chemical shift corresponding to product **3** (green circle in **Figure 5E**). The enzymatic conversion of hyperpolarized probe **2** was successfully monitored *in vivo*. When a mouse was pretreated with K579, the appearance of the product peak was significantly suppressed, indicating that the production of product **3** from ^{13}C-BCM-5 was mediated by DPP-IV *in vivo* (**Figure S8**). These results demonstrate the utility of our ^{13}C-labeling strategy for peptides to realize long T_1 for biological applications, even in a pentapeptide, whose molecular weight exceeds 500.
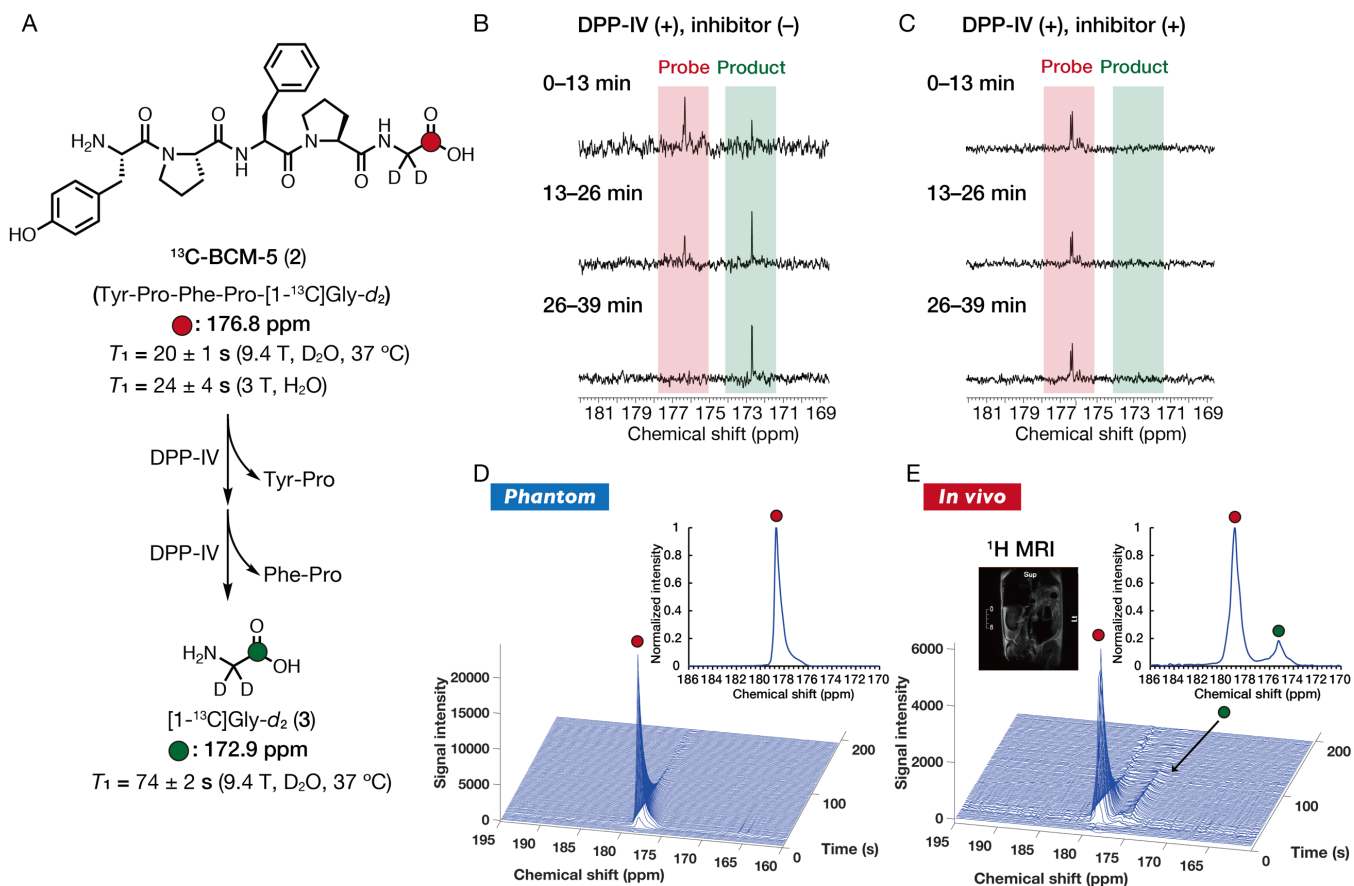
Figure 5. (A) Enzymatic reaction scheme of ^{13}C-BCM-5 (**2**) with DPP-IV to produce [1-^{13}C]Gly-d_2 (**3**). Colored atoms indicate isotope-enriched ^{13}C. ^{13}C chemical shift was determined by ^{13}C NMR measurements at 9.4 T. Since the cis/trans isomers of ^{13}C-BCM-5 give multiple ^{13}C NMR signals, the ^{13}C chemical shift of the major peak was shown. T_1 values at 9.4 T were measured using the saturation recovery method (9.4 T, D$_2$O, 37 ℃, pD = 7.4 ± 0.1). ^{13}C-BCM-5 (5 mM in D$_2$O) and [1-^{13}C]Gly-d_2 (10 mM in D$_2$O) were used for the measurements. The corrected T_1 at 3 T was calculated from the hyperpolarized signal decay. (B) and (C) *In vitro* ^{13}C NMR monitoring of DPP-IV-mediated enzymatic reaction without inhibitor (B) or with inhibitor (C). The ^{13}C NMR spectra were acquired at 9.4 T under the following conditions: ^{13}C-BCM-5 (5 mM) in 0.1 M phosphate buffer containing 1% DMSO (pH = 7.4, 37 ℃) with or without a DPP-IV inhibitor (K579) (0.1 mM). The final concentration of human DPP-IV was 6.7×10^2 units/L. (D) Dynamic ^{13}C MRS of hyperpolarized ^{13}C-BCM-5. 10 µL of ^{13}C-BCM-5 (*ca.* 0.85 M in H$_2$O) containing OX063 (*ca.* 11 mM) was hyperpolarized using Hypersense. Dissolution buffer was 3.5 mL of H$_2$O containing 200 mg/L EDTA disodium salt. 1.0 mL of hyperpolarized solution was added to a glass vial with 2.0 mL of H$_2$O containing 200 mg/L EDTA disodium salt. (E) *In vivo* observation of hyperpolarized ^{13}C-BCM-5. 60 µL of ^{13}C-BCM-5 (*ca.* 0.85 M in H$_2$O) containing OX063 (*ca.* 11 mM) was hyperpolarized using Hypersense. Repetition time = 1 s, flip angle = 10°, and the dissolution buffer was 3.5 mL of PBS containing 200 mg/L EDTA disodium salt. The spectra were acquired using a 3 T MRI scanner, following intravenous administration of 400 µL of hyperpolarized ^{13}C-BCM-5 into the tail vein. Insets are the summed ^{13}C MR spectrum and ^{1}H anatomical image of the mouse body, where ^{13}C MRS was performed. The colored circles indicating the hyperpolarized peaks correspond to ^{13}C atoms shown in (A). The reproducibility of (E) was confirmed (n = 3).

Development of ^{13}C-GSH as a tripeptide DNP NMR probe with a long T_1

Next, we applied our ^{13}C-labeling strategy to an essential biological peptide, GSH, to further demonstrate the potential utility of our strategy. GSH is a natural tripeptide composed of glutamic acid, cysteine, and glycine, and is involved in a broad range of biological phenomena as a non-protein thiol. The intracellular concentration of GSH reaches as high as 0.5–10 mM. GSH also plays important biological roles, such as conjugation of electrophiles, maintenance of intracellular redox states, and trapping oxidants.[47] Furthermore, decreased intracellular levels of GSH have been observed in several cancers and diabetes.[48] The intracellular uptake of GSH is generally regulated by several enzymes. The initial step is either hydrolysis or transpeptidation of the γ-glutamyl moiety mediated by γ-glutamyl transpeptidase (GGT) to produce Cys-Gly. Subsequent hydrolysis by dipeptidases produces Cys and Gly as enzymatic products (**Figure 6A**).[49,50] Thereafter, each amino acid component is transported into cells and used for intracellular biosynthesis of GSH. To date, there have been reports that detected the presence of GSH *in cells* or *in vitro* using fluorescent probes.[51–53] Furthermore, by injecting [2-^{13}C]Gly, biosynthesis of ^{13}C-incorporated GSH has been successfully observed in mice or patients using non-hyperpolarized ^{13}C MRS.[54,55] However, *in vivo* real-time monitoring of metabolism related to intracellular uptake of GSH, mediated by GGT and dipeptidases, has never been achieved.

To realize *in vivo* detection of GSH metabolism by DNP NMR, ^{13}C-GSH (γ-Glu-Cys-[1-^{13}C]Gly-d_2) was developed based on our ^{13}C-labeling strategy. ^{13}C-GSH was synthesized according to **Scheme S5**. The C-terminal carboxylic ^{13}C in ^{13}C-GSH showed a long T_1 of 52 ± 2 s (9.4 T, 10 mM, D$_2$O, 37 ºC, **Figure 6A and Table S6**). This long T_1 demonstrates the broad applicability of our ^{13}C-labeling strategy for peptides. Next, we conducted ^{13}C MRS of hyperpolarized ^{13}C-GSH using a 3 T MRI scanner (**Figure S9**). Hyperpolarized ^{13}C-GSH produced an enhanced ^{13}C MR signal. By fitting the hyperpolarized signal decays, the corrected T_1 was calculated to be 58 ± 3 s (3 T, H$_2$O). This corrected T_1 value of the C-terminal carboxylic ^{13}C of ^{13}C-GSH allows a sufficiently long hyperpolarization lifetime that is useful for *in vivo* analysis.

We then conducted *in vivo* analysis using hyperpolarized ^{13}C-GSH. After dissolution with PBS, hyperpolarized ^{13}C-GSH solution was intravenously administered to a healthy nude mouse (Athymic NCr-nu/nu). Dynamic ^{13}C MR spectra were acquired from the body region (**Figure 6B**). As a result, the hyperpolarized parental signal of ^{13}C-GSH was observed at the same chemical shift as in the *in vitro* phantom experiment using hyperpolarized ^{13}C-GSH (red circle in **Figure 6B**, **S9**). In addition, the product peak was observed at 175 ppm in the hyperpolarized ^{13}C spectra (green circle in **Figure 6B**). This new peak was characterized as [1-^{13}C]Gly-d_2 (**3**), a metabolic product of the ^{13}C-GSH probe, by comparison with the thermally equilibrated ^{13}C NMR of an authentic sample of [1-^{13}C]Gly-d_2 (**3**) at 9.4 T (**Figure S10**). To confirm whether the production of [1-^{13}C]Gly-d_2 (**3**) from ^{13}C-GSH was mediated by GGT, we pretreated a mouse with a GGT inhibitor, GGsTop® and performed ^{13}C MRS of the hyperpolarized ^{13}C-GSH probe *in vivo* (**Figure 6C**). The appearance of the product peak was significantly suppressed, indicating that the production of [1-^{13}C]Gly-d_2 (**3**) from ^{13}C-GSH was mediated by GGT. These results suggest the monitoring of the sequential enzymatic reactions of ^{13}C-GSH.
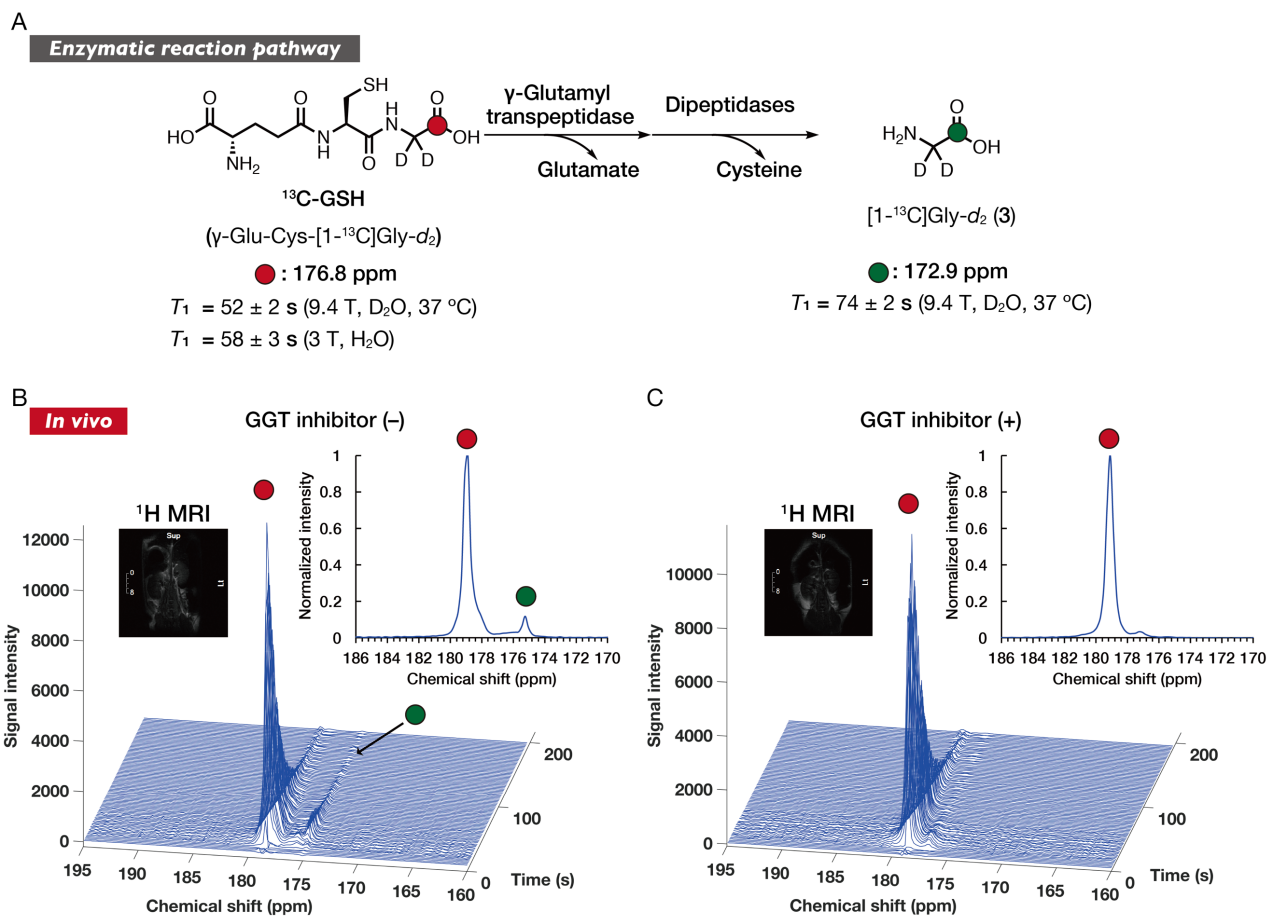
Figure 6. (A) Enzymatic reaction pathway of ^{13}C-GSH (γ-Glu-Cys-[1-^{13}C]Gly-d_2). Colored atoms indicate isotope-enriched ^{13}C. ^{13}C chemical shift was determined by ^{13}C NMR measurements at 9.4 T. T_1 values at 9.4 T were measured using the saturation recovery method (9.4 T, 10 mM, D$_2$O, 37 °C, pD = 7.4 ± 0.1). The corrected T_1 at 3 T was calculated from the hyperpolarized signal decay. (B) and (C) Dynamic ^{13}C MRS was performed in the body of a healthy nude mouse (Athymic NCr-nu/nu) without GGT inhibitor (B) or with GGT inhibitor (C). 35 μL of ^{13}C-GSH (*ca.* 1.8 M in H$_2$O) containing OX063 (*ca.* 19 mM) was hyperpolarized using Hypersense. Repetition time = 1 s, flip angle = 10°, and the dissolution buffer was 3.5 mL of PBS containing 200 mg/L EDTA disodium salt. A mouse was pretreated with GGsTop® (25 mg/kg) 0.5 h before the measurement in (C). The spectra were acquired using a 3 T MRI scanner, following intravenous administration of 400 μL of hyperpolarized ^{13}C-GSH into the tail vein. Insets are the summed ^{13}C MR spectrum and ^{1}H anatomical image of the mouse body, where ^{13}C MRS was performed. The colored circles indicating the hyperpolarized peaks correspond to ^{13}C atoms shown in (A). The reproducibility of (B) and (C) was confirmed (n = 3).

Conclusion

In this study, we proposed a ^{13}C-labeling strategy for the development of peptide-based DNP NMR molecular probes with long T_1 that is applicable to hyperpolarized *in vivo* studies. Focusing on the molecular structures of peptides, including main chains and side chains, experimental and computational T_1 relaxation analysis revealed that the C-terminal [1-^{13}C]Gly-d_2 residue is preferable for long T_1 in oligopeptides. Indeed, by utilizing the C-terminal [1-^{13}C]Gly-d_2 residue, we realized long T_1 in a pentapeptide, β-casomorphin-5, and a tripeptide, GSH, which is an important biological antioxidant. Finally, hyperpolarized ^{13}C-BCM-5 and ^{13}C-GSH enabled *in vivo* monitoring of enzymatic reactions, demonstrating the practical utility of our ^{13}C-labeling strategy.

The significance of this study is to demonstrate that long T_1 useful for DNP MR analysis can be realized even for large molecules if we investigate T_1 and R_1 based on the molecular structures. Because of the negative correlation between molecular weight and T_1, ^{13}C molecules with large molecular weights (> 200) have generally been considered impractical as DNP NMR molecular probes for biological applications. However, since the local motions of the molecule have significant effects on the relaxation of the observed nucleus, it is necessary to focus on the structures of molecules and to understand their dynamics. This study sheds light on the fact that a large molecular weight does not simply mean a short T_1 and that structure-based T_1 relaxation analysis is essential to realize long T_1 for DNP NMR probes (**Figure 7**).

Our ^{13}C-labeling strategy can realize long T_1 for oligopeptides and thus has the potential to expand the range of substrates for DNP NMR, especially for *in vitro* and *in vivo* hyperpolarized MR analyses that have not been offered thus far. This study also indicates the possibility that long T_1, applicable for biological hyperpolarized studies, can be achieved in large molecules other than peptides by conducting structure-based T_1 relaxation analysis. Although several attempts have been made to develop DNP NMR molecular probes by focusing on enzymatic parameters, biocompatibility, and other biochemical properties, one of the most crucial bottlenecks has been the short T_1 of substrates. Our ^{13}C-labeling strategy may pave the way for the use of molecules with large molecular weights as DNP NMR molecular probes with long T_1 for biomedical applications.
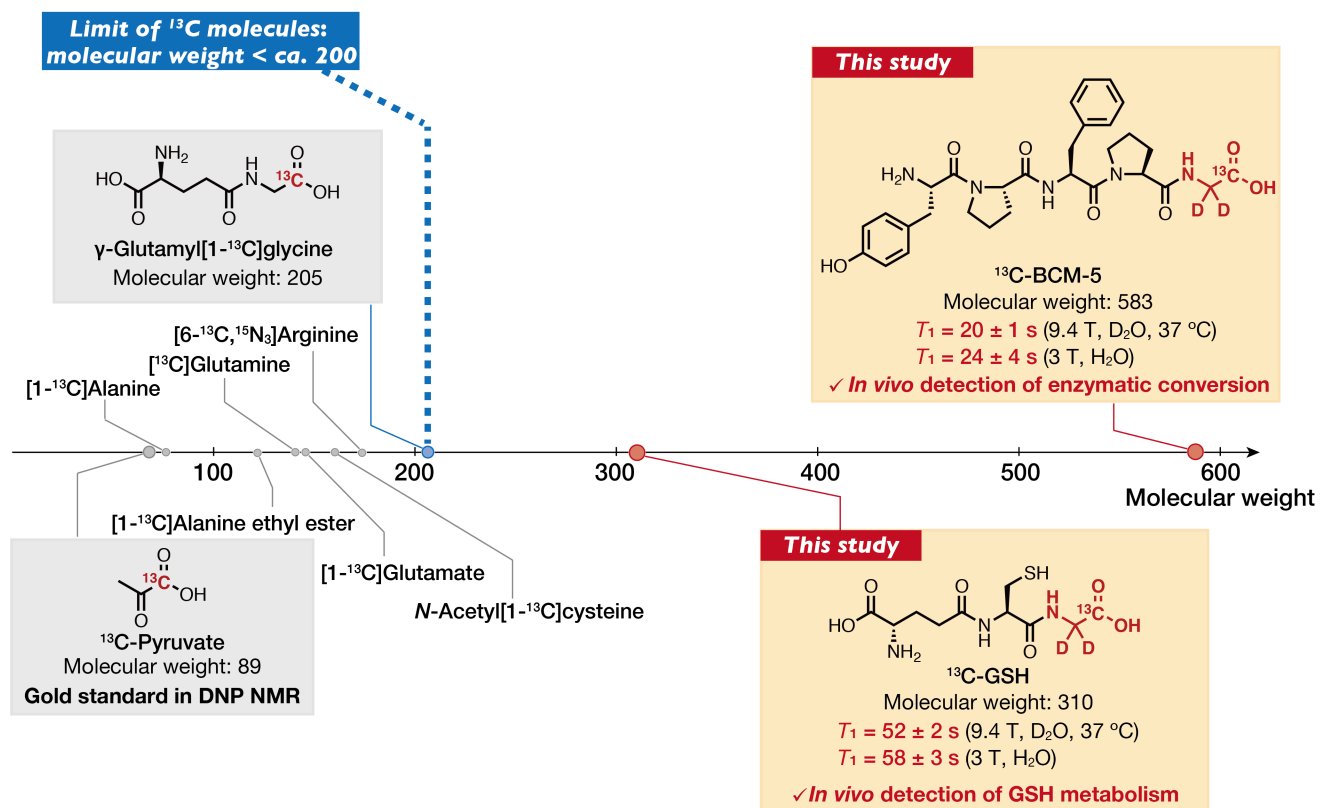
Figure 7. Schematic diagram illustrating the relationship between molecular weight and chemical structures of ^{13}C-pyruvate, ^{13}C-amino acids, and peptides that have been used for *in vivo* hyperpolarization MR studies, and the peptide-based DNP NMR molecular probes developed in this study.

Author Contributions

S.S. conceived and designed the project; Y.K. synthesized compounds with the help of Y.S., J.M., H.N., N.R., and R.S.; Y.K. conducted NMR measurements for relaxation analysis and other *in vitro* evaluations with the help of Y.S. and H.N.; K.Y., T.S., Y.T., A.E.E., F.H., M.M., and M.C.K. organized and/or performed the hyperpolarized experiments; K.M., W.M., and M.N. organized and/or performed the computational analysis; Y.K., Y.S., and S.S. wrote the manuscript, which was edited by all co-authors.

Conflicts of interest

There are no conflicts of interest to declare.

References

1. Ardenkjaer-Larsen, J. H. *et al*. Increase in signal-to-noise ratio of >10,000 times in liquid-state NMR. *Proc. Natl Acad. Sci. USA* **100**, 10158–10163 (2003).

2. Comment, A. Dissolution DNP for *in vivo* preclinical studies. *J. Magn. Reson.* **264**, 39–48 (2016).

3. Kurhanewicz, J. *et al.* Hyperpolarized ^{13}C MRI: path to clinical translation in oncology. *Neoplasia* **21**, 1–16 (2019).

4. Wang, Z. J. *et al.* Hyperpolarized ^{13}C MRI: state of the art and future directions. *Radiology* **291**, 273–284 (2019).

5. Gabellieri, C. *et al.* Therapeutic target metabolism observed using hyperpolarized ^{15}N choline. *J. Am. Chem. Soc.* **130**, 4598–4599 (2008).

6. Nonaka, H. *et al.* A platform for designing hyperpolarized magnetic resonance chemical probes. *Nat. Commun.* **4**, 2411 (2013).

7. Durst, M. *et al.* α-Trideuteromethyl[15N]glutamine: A long-lived hyperpolarized perfusion marker. *Magn. Reson. Med.* **76**, 1900–1904 (2016).

8. Nonaka, H. *et al.* Design of a ^{15}N molecular unit to achieve long retention of hyperpolarized spin state. *Sci. Rep.* **7**, 40104 (2017).

9. Gamliel, A. *et al.* Hyperpolarized [^{15}N]nitrate as a potential long lived hyperpolarized contrast agent for MRI. *J. Magn. Reson.* **299**, 188–195 (2019).

10. Doura, T., Hata, R., Nonaka, H., Ichikawa, K. & Sando, S. Design of a ^{13}C magnetic resonance probe using a deuterated methoxy group as a long-lived hyperpolarization unit. *Angew. Chem. Int. Ed.* **51**, 10114–10117 (2012).

11. Allouche-Arnon, H. *et al. In vivo* magnetic resonance imaging of glucose - initial experience. *Contrast Media Mol. Imaging* **8**, 72–82 (2013).

12. Rodrigues, T. B. *et al.* Magnetic resonance imaging of tumor glycolysis using hyperpolarized ^{13}C-labeled glucose. *Nat. Med.* **20**, 93–97 (2014).

13. Hundshammer, C. *et al.* Deuteration of hyperpolarized ^{13}C-labeled zymonic acid enables sensitivity-enhanced dynamic MRI of pH. *ChemPhysChem* **18**, 2422–2425 (2017).

14. Imakura, Y. *et al.* Rational design of [^{13}C,D$_{14}$]*tert*-butylbenzene as a scaffold structure for designing long-lived hyperpolarized ^{13}C probes. *Chem. Asian J.* **13**, 280–283 (2018).

15. Taglang, C. *et al.* Late-stage deuteration of ^{13}C-enriched substrates for T_1 prolongation in hyperpolarized ^{13}C MRI. *Chem. Commun.* **54**, 5233–5236 (2018).

16. Becker, E. D., Shoup R. R. & Farrar, T. C. ^{13}C NMR spectroscopy: relaxation times of ^{13}C and methods for sensitivity enhancement. *Pure Appl. Chem.* **32**, 51–66 (1972).

17. A. Abragam, *Principles of Nuclear Magnetism*, (Oxford Univ. Press, Oxford, 1961).

18. Bloembergen, N., Purcell, E. M. & Pound, R. V. Relaxation effects in nuclear magnetic resonance absorption. *Phys. Rev.* **73**, 679–712 (1948).

19. Keshari, K. R. & Wilson, D. M. Chemistry and biochemistry of ^{13}C hyperpolarized magnetic resonance using dynamic nuclear polarization. *Chem. Soc. Rev.* **43**, 1627–1659 (2014).

20. Kondo, Y., Nonaka, H., Takakusagi, Y. & Sando, S. Design of nuclear magnetic resonance molecular probes for hyperpolarized bioimaging. *Angew. Chem. Int. Ed.* **60**, 14779–14799 (2021).

21. Abusalim, J. E. *et al.* Simple Esterification of [1-^{13}C]-Alpha-Ketoglutarate Enhances Membrane Permeability and Allows for Noninvasive Tracing of Glutamate and Glutamine Production. *ACS Chem. Biol.* **16**, 2144–2150 (2021).

22. Nishihara, T. *et al.* Direct monitoring of γ-glutamyl transpeptidase activity in vivo using a hyperpolarized ^{13}C-labeled

molecular probe. *Angew. Chem. Int. Ed.* **55**, 10626–10629 (2016).

23. Petsalaki, E. & Russell, R. B. Peptide-mediated interactions in biological systems: new discoveries and applications. *Curr. Opin. Biotechnol.* **19**, 344–350 (2008).

24. Yamamoto, K. *et al.* Real-Time insight into in vivo redox status utilizing hyperpolarized [1-^{13}C] *N*-acetyl cysteine. *Sci. Rep.* **11**, 12155 (2021).

25. Jensen, P. R., Karlsson, M., Meier, S., Duus, J. & Lerche, M. H. Hyperpolarized amino acids for in vivo assays of transaminase activity. *Chem. Eur. J.* **15**, 10010–10012 (2009).

26. Cho, A., Eskandari, R., Granlund, K. L. & Keshari, K. R. Hyperpolarized [6-^{13}C,^{15}N$_3$]-Arginine as a Probe for *in Vivo* Arginase Activity. *ACS Chem. Biol.* **14**, 665–673 (2019).

27. Gallagher, F. A., Kettunen, M. I., Day, S. E., Lerche, M. & Brindle, K. M. ^{13}C MR spectroscopy measurements of glutaminase activity in human hepatocellular carcinoma cells using hyperpolarized ^{13}C-labeled glutamine. *Magn. Reson. Med.* **60**, 253–257 (2008).

28. Salamanca-Cardona, L. *et al. In vivo* imaging of glutamine metabolism to the oncometabolite 2-hydroxyglutarate in IDH1/2 mutant tumors. *Cell Metab.* **26**, 830–841 (2017).

29. Cabella, C. *et al. In vivo* and *in vitro* liver cancer metabolism observed with hyperpolarized [5-^{13}C]glutamine. *J. Magn. Reson.* **232**, 45–52 (2013).

30. Gallagher, F. A. *et al.* Detection of tumor glutamate metabolism in vivo using ^{13}C magnetic resonance spectroscopy and hyperpolarized [1-^{13}C]glutamate. *Magn. Reson. Med.* **66**, 18–23 (2011).

31. Chen, J., Hackett, E. P., Singh, J., Kovács, Z. & Park, J. M. Simultaneous Assessment of Intracellular and Extracellular pH Using Hyperpolarized [1-^{13}C]Alanine Ethyl Ester. *Anal. Chem.* **92**, 11681–11686 (2020).

32. Wilson, D. M. *et al.* Generation of hyperpolarized substrates by secondary labeling with [1,1-^{13}C] acetic anhydride. *Proc. Natl. Acad. Sci. USA* **106**, 5503–5507 (2009).

33. Miyanishi, K. *et al.* Prediction of ^{1}H singlet relaxation via intermolecular dipolar couplings using the molecular dynamics method. Preprint available at http://arxiv.org/abs/arXiv:2110.10488 (2021).

34. Levy, G. C. Carbon-13 spin-lattice relaxation studies and their application to organic chemical problems. *Acc. Chem. Res.* **6**, 161–169 (1973).

35. Breitmaier, E., Spohn, K. H. & Berger, S. ^{13}C Spin-lattice relaxation times and the mobility of organic molecules in solution. *Angew. Chem. Int. Ed.,* **14**, 144–159 (1975).

36. Kuhlmann, K. F. & Grant, D. M. The nuclear overhauser enhancement of the carbon-13 magnetic resonance spectrum of formic acid. *J. Am. Chem. Soc.* **90**, 7355–7357 (1968).

37. Levy, G. C., Cargioli, J. D. & Anet, F. A. L. Carbon-13 Spin-Lattice Relaxation in Benzene and Substituted Aromatic Compounds. *J. Am. Chem. Soc.* **95**, 1527–1535 (1973).

38. Gust, D., Pearson, H., Armitage, I. M. & Roberts, J. D. Nuclear magnetic resonance spectroscopy. Spin-lattice relaxation of the acetic acid carboxyl carbon. *J. Am. Chem. Soc.* **98**, 2723–2726 (1976).

39. Alger, T. D. *et al.* Carbon-13 spin-lattice relaxation in condensed aromatic compounds. *J. Phys. Chem.* **84**, 632–636 (1980).

40. Wong, T. C., Ang, T. T., Guziec F. S. & Moustakis, C. A. The chemical-shift anisotropy mechanism in ^{77}Se spin-lattice relaxation. Measurement of ^{77}Se T_1 at several magnetic fields. *J. Magn. Reson.* **57**, 463–470 (1984).

41. Sakaguchi, M., Koseki, M., Wakamatsu, M. & Matsumura, E. Effects of systemic administration of β-casomorphin-5 on learning and memory in mice. *Eur. J. Pharmacol.* **530**, 81–87 (2006).

42. Jarmołowska, B. *et al.* Serum activity of dipeptidyl peptidase IV (DPPIV; EC 3.4.14.5) in breast-fed infants with symptoms of allergy. *Peptides* **28**, 678–682 (2007).

43. Aertgeerts, K. N-linked glycosylation of dipeptidyl peptidase IV (CD26): Effects on enzyme activity, homodimer formation, and adenosine deaminase binding. *Protein Sci.* **13**, 145–154 (2004).

44. Onoyama, H. *et al.* Rapid and sensitive detection of early esophageal squamous cell carcinoma with fluorescence probe targeting dipeptidylpeptidase IV. *Sci. Rep.* **6**, 26399 (2016).

45. Yu, D. M. T. *et al.* The dipeptidyl peptidase IV family in cancer and cell biology. *FEBS J.* **277**, 1126–1144 (2010).

46. Pro, B. & Dang, N. H. CD26/dipeptidyl peptidase IV and its role in cancer. *Histol. Histopathol.* **19**, 1345–1351 (2004).

47. Lushchak, V. I. Glutathione homeostasis and functions: Potential targets for medical interventions. *J. Amino Acids* **2012**, 1–26 (2012).

48. Townsend, D. M., Tew, K. D. & Tapiero, H. The importance of glutathione in human disease. *Biomed. Pharmacother.* **57**, 145–155 (2003).

49. Zhang, H., Forman, H. J. & Choi, J. γ-Glutamyl transpeptidase in glutathione biosynthesis. *Methods Enzymol.* **401**, 468–483 (2005).

50. Bachhawat, A. K. & Yadav, S. The glutathione cycle: Glutathione metabolism beyond the γ-glutamyl cycle. *IUBMB Life* **70**, 585–592 (2018).

51. Chen, X., Zhou, Y., Peng, X. & Yoon, J. Fluorescent and colorimetric probes for detection of thiols. *Chem. Soc. Rev.* **39**, 2120–2135 (2010).

52. Jung, H. S., Chen, X., Kim, J. S. & Yoon, J. Recent progress in luminescent and colorimetric chemosensors for detection of thiols. *Chem. Soc. Rev.* **42**, 6019–6031 (2013).

53. Niu, L. Y. *et al.* Design strategies of fluorescent probes for selective detection among biothiols. *Chem. Soc. Rev.* **44**, 6143–6160 (2015).

54. Thelwall, P. E. *et al.* Noninvasive *in vivo* detection of glutathione metabolism in tumors. *Cancer Res.* **65**, 10149–10153 (2005).

55. Skamarauskas, J. T. *et al.* Noninvasive *in vivo* magnetic resonance measures of glutathione synthesis in human and rat liver as an oxidative stress biomarker. *Hepatology* **59**, 2321–2330 (2014).